A Hybrid Prediction Fault Location Model for Copper Wire Manufacturing Process

Robert Agyare Ofosu[1], Huangqiu Zhu[1]*, Benjamin Odoi[2]

[1]School of Electrical and Information Engineering, Jiangsu University, Zhenjiang 212013, China, e-mail: raofosu@umat.edu.gh; zhuhuangqiu@ujs.edu.cn

[2]Faculty of Engineering, University of Mines and Technology, WT-0038-7367, Tarkwa, Ghana, e-mail: bodoi@umat.edu.gh

Abstract: This paper presents a novel prediction of fault location during copper wire manufacturing using a hybrid Nonlinear Autoregression Neural Network (NARNN) and Markov chain model. A four (4) year daily primary data spanning from 2018 to 2022 consisting of 261502 data points obtained from a cable manufacturing company in Ghana was used for the prediction. A comparison between the suggested model and decision tree algorithm was done. To assess the predictive effectiveness of the two models, performance indicators including Mean Absolute Deviation (MAD), Root Mean Square Error (RMSE), and Mean Absolute Percentage Error (MAPE) were used. As determined by their evaluation criteria, the findings revealed that the suggested hybrid model had superior data fitting and accurate prediction capabilities.

Keywords: tension; prediction; wire breaks; fault location; NARNN; decision tree; markov chain model

1 Introduction

Electrical cables are made all over the world due to their widespread use. Basically, electrical cables are current-conducting wires either copper or aluminum that have been twisted, braided, or bonded into a single assembly with or without insulation. They are employed specifically for the transmission of electrical or telecommunication signals. Electrical cables are necessary because they serve as the foundation for the functionality of all electrical equipment. To produce cables that are of good quality, a number of production processes must be used. One of these essential manufacturing processes is the drawing stage, which entails drawing a copper or aluminum rod through a series of progressively smaller synthetic diamond or tungsten carbide dies. Drawing reduces the rod to a wire with the required diameter that has great surface quality and enhanced mechanical qualities like strength and hardness [1]-[3].

A typical copper rod is drawn in four steps. These include unwinding, drawing, annealing and rewinding. The thick copper rod is unwound at the payoff drive to the diesing chamber during the unwinding phase. The ultimate wire diameter is produced in the diesing chamber by forcing the thick copper wire through a sequence of progressively smaller dies. Lubricant, like oil, is circulated in the diesing chamber to lower friction and wire wear. The drawn copper wire is put through a specific heat treatment in the annealing chamber to soften it and increase its malleability. A dancer system is also mounted between the payoff and take-up drives so as to sense and regulate the wire tension to the desired limit. The drawn wire is evenly coiled onto a bobbin at the take-up with the aid of the traverse. A counter installed on the moving web next to the dancer provides data on the length of wire wound onto the bobbin. Figure 1 depicts the process of copper wire drawing [4].

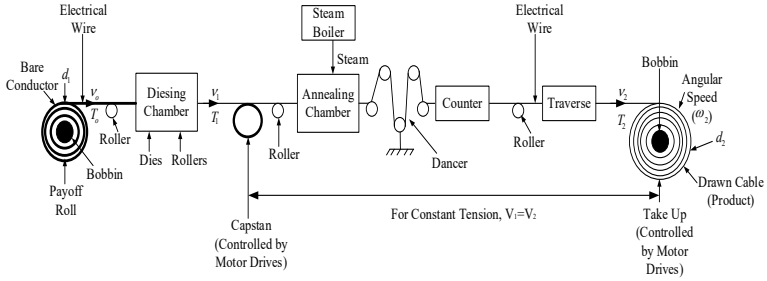

Figure 1
Copper wire drawing process schematic diagram

where, d_1 is the wire's initial diameter before drawing, d_2 is actual wire's diameter upon drawing, $V_0=V_1$ is line speed of pay-off or capstan, V_2 is line speed of take up, $T_0=T_1$ is torque of payoff or capstan, T_2 is torque of take up, ω_2 is angular speed of take-up drive

After the wires are drawn, they are bundled to form a cable, which is then extruded with insulating polymers such as Cross-Linked Polyethylene, Polyethylene, and Polyvinyl Chloride. Extrusion is an important stage in the production line since it inhibits copper losses in cables and protects the conductor from physical harm and environmental hazards. After extrusion, the final product is ready for market consumption after passing quality control tests [3], [5]. Among the most crucial things to take into consideration in the cable manufacturing sector is the final resistance or diameter of the wire, which should not differ substantially from the standard after production. That is, the wire's tension should remain consistent during the drawing stage of the cable production process so that the wire's diameter or cross-sectional area remains unchanged. Failure to ensure this can lead to fire outbreaks that could kill innocent lives and destroy millions of properties as a result of heat generation when substandard wires or cables are used [6]. According to research, tension variation during the wire drawing process is

primarily caused by faults in the drawing machines' components. In most cases, this causes machines to abruptly stop, resulting in wire breaks caused by stretching the wire beyond its tensile strength [7], [8].

Similarly, in the event of a fault, determining the exact location of the fault in wire drawing machines is always a bigger challenge for the experts who work on these machines, as it usually takes much longer to locate the faults in order to restore them. Most cable manufacturing industries face significant challenges as a result of this phenomenon, which causes increased downtime, production losses, energy waste, and scrap production [9]. Several factors contribute to wire tension and breakage during the drawing process. Low drawing or annealing solution concentration, entanglement in the basket, bad or copper dust in dies, annealing bearing failure, improper drive and tensioner setting, oxidation of wire due to bad steam flow in the annealer, power outage, torque or speed variation due to changes in roll diameter between the payoff drive and the take-up drive among other factors. These faults are mostly located in the drawing chamber, annealing chamber, capstan, recirculatory system, dancer, payoff, take-up, AC drive and traverse. Therefore, developing a model that can predict the location of faults during the copper wire drawing process is necessary in order to avert these challenges.

Several models for fault prediction have been reported in the literature. These models are categorized as statistical, physical, and artificial intelligence models [10]. Physical models suffer from multiple iterations before achieving the desired results. Furthermore, these models demand a significant amount of reliable data [11]. Seasonal Autoregressive Integrated Moving Average (SARIMA), Auto-Regressive Moving Average (ARMA), Generalized Autoregressive Conditional Heteroscedasticity (GARCH) and Auto-Regressive Integrated Moving Average (ARIMA) are the most frequently employed statistical models [12]. It has been demonstrated that these models can predict if the time series data exhibit a linear relation. Their strength is based on historical data. However, because statistical models have several transitory periods and large variability, they are unable to produce reliable predictions for time series with nonlinearities, such as the wire break location prediction in the drawing machines [13].

Artificial Intelligence (AI) models such as Support Vector Machine (SVM), Logistic Regression (LR), Adaptive Neuro Fuzzy Inference System (ANFIS), Artificial Neural Networks (ANNs), Decision Trees, Fuzzy Logic, and k-Means are well recognized for their capacity to resolve a nonlinear time series with greater precision and have produced favorable outcomes in the creation of extremely precise fault diagnostic systems [14-19]. Among the AI techniques, ANN is one of the most popular and several studies have shown that it outperforms other techniques [20], [21]. The advantages of ANN are enormous because it is fault-tolerant, can learn sophisticated nonlinear relationships, and has powerful classification attributes. Besides, due to the non-parametric nature of ANN prediction, having process knowledge of the production of the time series is

not necessary. Furthermore, once trained, ANNs are capable of making accurate predictions [22]. Nonetheless, ANN lack coherence, leading to their inappropriateness for deployment in instances under which it is essential to determine which elements did contribute to a technical fault [21], [22].

There are various subcategories of ANN. These include Radial Basis Function Neural Network (RBFNN), Backpropagation Neural Network (BPNN), Recurrent Neural Network (RNN), Generalized Regression Neural Network (GRNN), and Nonlinear Autoregressive Neural Network (NARNN). Because the prediction of wire break location in the cable manufacturing process involves fluctuating parameters that are highly nonlinear and complex, research has shown that NARNN has the capability to predict the dynamics of this complex system with high precision and quick convergence [23], [24]. NARNN has been utilized successfully in a variety of applications for fault prediction. Some of which include transformer oil dissolved gas concentration [12], fault prediction in software [25], rolling element bearing deterioration prediction [26], prediction of infiltration of underground water by hydraulic fluid leaks [27], engine fault detection and failure prediction in the manufacturing process [28], [29], passenger flow forecasting [30], meteorological time series forecasting [31], [32], Heating Ventilation and Air Conditioning (HVAC) predictions [23], [33] geomagnetic fluctuations prediction [34], prediction of COVID-19 cases [35] among other complex dynamical systems.

To the author's best knowledge, the hybrid NARNN-Markov chain model has never been used to predict fault location in wiring drawing machines and no literature has ever reported on the prediction of wire breaks and fault location in drawing machines during copper wire drawing in the cable manufacturing industries. As a result, this paper proposed a novel approach to accurately classify and locate the probability of wire breaks in the copper wire drawing process by combining NARNN with a Markov chain model. To determine the model's effectiveness in fault location, a comparative analysis was performed using the decision tree algorithm. The findings clearly show the proposed models' effectiveness in predicting fault locations. Therefore, it is anticipated that this research can be the basis for the deployment of corrective maintenance in the cable manufacturing industry. Thus, the operators can anticipate potential fault locations and implement recommended preventive measures.

1.1 Nonlinear Autoregressive Neural Network

The Nonlinear Autoregression Neural Network (NARNN) blends neural network techniques' capacity for matching nonlinear function with that of autoregressive methods for unearthing probable time series sources [12], [32]. The architecture is developed and provided with training in an open loop, with the intended target variables making up the feedback loop to ensure higher training accuracy.

The configuration is changed to a closed loop after learning, and the estimated outputs are utilized as new signals acting as feedback to the network. The NARNN is a nonlinear, discrete, autoregressive model used in forecasting time series data expressed as [26], [27]:

$$y(t) = h(y(t-1),\ y(t-2) + ... + y(t-d)) + \varepsilon(t) \tag{1}$$

where *y(t)* is prediction's outcome at a discontinuous step time *t* of the time series *y*, the series' past data is denoted by *d*, *ε(t)* symbolizes the series y's deviation at time step *t* and h connotes a hypothetical nonlinear quantity that the feedforward part of a neural network can predict while being trained.

The aim for training a neural network is to estimate the functional h(.) by maximizing the bias and weights of the network. As a result, the NARNN model is well-defined by Eq. (2) [26], [27].

$$y(t) = a_0 + \sum_{j=1}^{k} a_j \phi\left(\sum_{i=1}^{a} \beta_{ij} y(t-i) + \beta_{oj} \right) + \varepsilon(t) \tag{2}$$

where *a* depicts the entry number, *k* denotes the hidden layer's quantity containing activation function ϕ, variable β_{ij} determines how strongly the input layer *i* and the hidden layer *j* are connected. The values for the output and hidden layer, respectively, are a_o and β_{oj}, a_j is the connecting weight linking the output and the hidden layer.

The boosting of the NARNN model's architecture necessitates the identification of the quantity of hidden layers, time delays, and activation function, as well as a suitable learning technique. The desirable amount of time delay and hidden layers is determined by experiment. On the basis of Dandy and Maier, the activation function is selected. Finally, due to their accuracy and high convergence speed, Bayesian regularization algorithms and the Levenberg-Marquardt are utilized to train the model [26], [27]. Generally, the input data quality, universality and size, as well as proper model development and assessment, are critical to the successful application of NARNN models [28], [29].

1.2 Decision Tree Method

A kind of supervised learning is the decision tree approach. It is one of the most widely used classification techniques due to its high accuracy and low computational cost. Its flexibility, nonparametric nature, and capacity to deal with nonlinear relationships between features and classes make it suitable for fault classification [36]. The decision-rules model's tree structure formation is based on if/else instructions. In theory, an iterative binary partition approach is used for the desired output to supervise the training sets. To divide the sample space, successive queries with yes/no options are posed. The locations in which the items

are examined are referred to as nodes. The test findings are subsequently relayed to a branch.

A decision tree has three different kinds of nodes. These include the internal nodes, leaf nodes, and root nodes. The test's result is based on each node's purity. After achieving the optimum value of purity, the node is terminated. The optimum value is established if a node only produces one kind of output. When classifying new samples, the decision tree and an item quantity will be examined. The chain of attribution from the root node to the leaf node maintains group forecast for the tested samples. The basic procedure in creating a decision tree is to identify the attribute that will be evaluated on a node, and an ancillary node to that node. Splitting refers to the entire process of identifying test and branch.

The process of splitting reduces the dataset's impurity that corresponds to class at a subsequent point. The task necessitates the computation of information gain, which is divided into entropy and the entropy splitting index. An indicator of entropy or impurity *i(t)* at a given node *t*, represents the entropy index as shown in Eq. (3) [37].

$$i(t) = -\sum_{j=1}^{k} p(w_j \mid t) \log p(w_j \mid t) \tag{3}$$

where $p(w_j \mid t)$ denotes the pattern's proportion assigned to a kind at node t.

The optimal splitting basic values x_j^R for the variable x_j are used to segregate a node that has not terminated into right child nodes tR and left child node tL. P_R and P_L make up the equivalent fractions of the new entities. Eq. (4) optimizes the difference by providing the most efficient entropy splitting index.

$$\Delta i(t) = i(t_p) - P_R i(t_L) - P_L i(t_R) \tag{4}$$

1.3 Markov chain Model

One variety of stochastic process is the Markov chain, which is widely used to analyze dynamic systems. The process is random, in which any future data exists in the current state. Furthermore, the probability and state transition matrix are important elements in implementing the Markov chain model. Unlike similar predictive techniques, the Markov chain model is simple to implement and neither does it necessitate a profound comprehension of changes in system dynamics. As a result, it is comparably simple to comprehend the data [38]. The Markov chain approach consists of five stages [38], [39]. The stages are:

Stage 1) Process state definition for the Markov chain.

Stage 2) Develop the state transition probability, P and state transition matrix, N. The Markov chain's state transition matrix, N, denotes the measured number of times of switching between states, as demonstrated in Eq. (5).

$$N = \begin{bmatrix} n_{11} & \cdots & n_{1s} \\ \vdots & \ddots & \vdots \\ n_{s1} & \cdots & n_{ss} \end{bmatrix} \tag{5}$$

n_{ij} indicates the amount of sequential transitions between states i and j

Suppose P represents a transition matrix that expresses all of the Markov chain model's transition probabilities for each state. P can therefore written as;

$$P = \begin{bmatrix} p_{11} & \cdots & p_{1s} \\ \vdots & \ddots & \vdots \\ p_{s1} & \cdots & p_{ss} \end{bmatrix}, i, j \in I \tag{6}$$

Then,

$$P\{X_{t+1} = j \mid X_t = i\} = p_{ij} \tag{7}$$

The probability of one step is described by Eq. (7). A homogenous Markov chain refers to transition probabilities that change independently with time *t*.

Therefore,

$$P\{X_{t+1} = j \mid X_t = i\} = P\{X_1 = j \mid X_0 = i\} = p_{ij} \tag{8}$$

Non-negative entries in each row summing up to unity are required by the matrix P. Hence,

$$0 \le p_{ij} \le 1 \text{ and } \sum_{j=1}^{t} p_{ij} = 1, \ \sqrt{i} \in I \tag{9}$$

State *i* to state *j* in k-steps probability of state transition is defined by Eq. (10).

$$p_{ij}(k) = P\{X_{n+k} = j \mid X_n = i\}, \ \sqrt{k} > 0, n \ge 0, \ \text{i}, j \in I \tag{10}$$

Eq. (11) describes the transition matrix P.

$$P(n) = P^{n-1} \times P = P^n \tag{11}$$

Stage 3) Ergodic Markov chain validation.

The constrained distribution's occurrence in an ergodic Markov chain must be confirmed by categorizing the P's state. The three parts are the irreducible Markov chain, the periodicity Markov chain, and the recurrent and transitory states.

Step 4) Probability values of Markov process

For probability values of Markov process, it is possible to calculate the mean return time and stationary probability distribution. For an ergodic Markov chain, the maximum allocation for a stationary probability distribution exists and is represented as:

$$\pi_j = \lim_{n \to 0} P(X_n = j \mid X_0 = i) \tag{12}$$

Thus

$$\pi_j = P_j(n) = \sum_k P_k(n-1)P_{kj} \text{ becomes } \pi j = \sum_k \pi_k P_{kj}, \quad \text{as n} \to \infty \text{ for j=0, 1,2,....} \tag{13}$$

Step 5) Model validation and Forecasting

To compute the forecasts, the base probability and state transition probability can be employed through Eq. (14).

$$P(S_j) = \sum_{i=1}^{n} P(S_i)P_{ij} \tag{14}$$

where P_{ij} depicts state transition probability and $P(S_i)$ the base probability.

Based on the assumption of independence, the Markov chain's authenticity is examined using the Chi-square test during the model validation process as shown in Eq. (15) [40].

$$X^2_{calculated} = \sum \frac{(Observed - Expected)}{Expected} \tag{15}$$

If $X^2_{calculated}$ is higher than $X^2_{tabulated}$ on the 0.05 crucial zones, the null hypothesis is refuted.

1.4 Error Metrics

The training and testing errors were used to assess the fitness and performance of prediction of the NARNN and decision tree models. The errors were evaluated using three indices: Mean Absolute Deviation (MAD), Root Mean Square Error (RMSE), and Mean Absolute Percentage Error (MAPE) [41], [42].

1.4.1 Root Mean Square Error

The test of the dispersion of predicted errors over real data sets is the Root Mean Square Error (RMSE). In other words, the RMSE elucidates how close an estimated model's forecasted values are to the actual data points. The formula is given as:

$$RMSE_{forecast} = \sqrt{\sum_{i=1}^{n} \left(\frac{Y_t - \hat{Y}_t}{n} \right)^2} \tag{16}$$

where $\hat{Y}_t$ indicates the prediction, Y_t the real data sets, and n the size of the sample.

1.4.2 Mean Absolute Percentage Error

The Mean Absolute Percentage Error (MAPE) is a percentage size measurement of a forecast's error. It is used to evaluate forecast accuracy and is expressed as:

$$MAPE_{forecast} = \left(\frac{1}{n} \sum \frac{\left| Y_t - \hat{Y}_t \right|}{\left| Y_t \right|} \right) \times 100\% \tag{17}$$

1.4.3 Mean Absolute Deviation

Mean Absolute Deviation (MAD) is the most fundamental indicator of prediction performance. MAD describes how large an error from the estimation is anticipated on mean as described by Eq. (18).

$$MAD = \left(\frac{1}{n} \sum \left| Y_t - \hat{Y}_t \right| \right) \tag{18}$$

The following is a discussion of the remaining sections: Section 2 explains the research approach, including data collection and preparation, the utilization of hybrid NARNN and Markov Chain model on the data and assessing the model's efficiency using statistical metrics. Explanation of the findings are given in Section 3. Section 4 concludes with some quick observations and suggestions.

2 Methods Used

2.1 Data Collection

A four-year period of daily primary data spanning 2018 to 2022 consisting of wire diameter (mm), length (m), number of spools, total length (km), number of wire breaks, and wire break rate as the independent variables and location of wire breaks as the dependent variable with a total data point of 261502 for each of the variables was used for the study. This data was taken at the wire drawing machines in a cable manufacturing industry in Ghana. The data was merged, cleaned, and organized for the analysis process.

2.2 Hybrid NARNN and Markov Chain Construction

The implementation process for the NARNN model is shown methodically in the flowchart in Figure 2. To start, during the data pre-processing stage, the simulation's data was partitioned into training (80%) and testing (20%) datasets.

The NARNN weights and bias were subsequently initialized with random numbers. Every iteration of their values was adjusted using Levenberg–Marquardt Back-Propagation (LMBP). The goal was to attain a target error with the fewest possible iterations. The last phase involves assessing the NARNN's performance and predicting capacity using the test data.

To predict the fault location on the basis of the output of NARNN, the performance is evaluated based on their probabilities. Figure 3 depicts the prediction stage of the located faults during the wire drawing stage of the cable manufacturing process. The variables *y(t-1), y(t-2), y(t-3) and y(t-4)* represents the input variables for instance the total wire length, number of spools, number of wire breaks and wire break rate. The location of wire breaks such as the drawing chamber, annealing chamber, dancer, and capstan, among others, is represented by the predicted output *y(t)*.

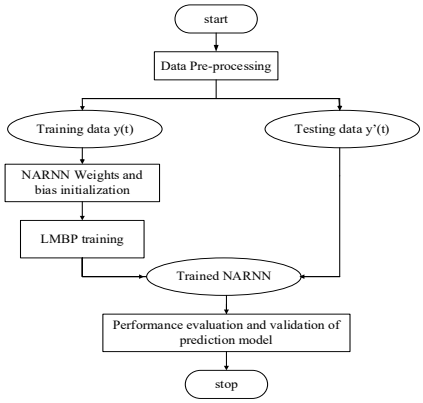

Figure 2
Flowchart of NARNN Model

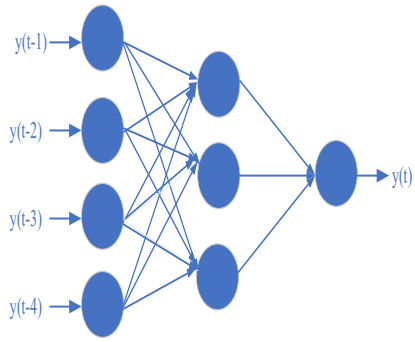

Figure 3
Fault Location Model of the NARNN

After the NARNN had classified the various faults, the Markov chain model was used to predict the probabilities of the faults occurring within a given location and the probability of faults occurring in other locations based on their pivot points. Firstly, the number of faults occurring within a given location was converted into a transitional matrix. Afterwards, a discrete-time Markov chain was created. The results of the Markov chain prediction were then displaced in the form of a chain displaying their transitional probabilities at various locations.

2.3 Construction of the Decision Tree Algorithm

The construction of the decision tree algorithm was achieved using Minitab Statistical Software version 21.1.0 after the dataset was loaded into the software. A decision tree plot and other statistical parameters were then recorded.

2.4 Simulations

The NARNN-Markov chain model and decision tree algorithm were checked for relevance, robustness, and inaccuracies using simulations of the dependent and independent variables. Owing to the NARNN's lack of interpretability of the fault location, the Markov chain was used to predict the probability of fault locations.

3 Results and Discussion

3.1 Exploratory Analysis

A summary of the variables taken into consideration in this research is shown in the Table 1. The average values of the variables considered in the descriptive statistics are given by 13583, 7.6646, 99.32, 0.7834, and 14.02 for length, number of spools, total length, number of wire breaks, and break rate, respectively. The Standard Error of the Mean (SE Mean) was also 192, 0.0819, 2.61, 0.0252, and 0.850 for length, number of spools, total length, number of wire breaks, and break rate. The smaller the standard error, the lower the risk. Likewise, the kurtosis was also reported as 126.66, 0.35, 694.37, 6.43, and 171.88 respectively for length, number of spools, total length, number of wire breaks, and break rate. From a statistical point of view, the variance is not constant, hence the data is heteroskedastic based on the kurtosis of the variables length, total length, number of wire breaks, and break rate being greater than 3.

Table 1
Exploratory Data Analysis

Variable	Mean	Standard Error of Mean	Kurtosis
Length	13583	192	126.66
Number of spools	7.6646	0.0819	0.35
Total length	99.32	2.61	694.37
Number of wire breaks	0.7834	0.0252	6.42
Break rate	14.02	0.850	171.88

3.2 Statistics of Faults at Various Locations

The statistics of wire breaks at various drawing machine locations between 2018 and 2022 are displayed in Figure 4. From the collected data, it can be seen that the drawing chamber had the highest number of wire breaks of 763. This was closely

followed by the capstan with 339 wire breaks. The next significant wire break was observed in the annealing chamber, with 276 wire breaks in this location. The number of unspecified wire break locations was reported as 475. Among all this break locations, the traverse was observed to be the list with a value of 1. The data unambiguously demonstrates that, as is typically found in most cable manufacturing companies, the drawing chamber, capstan, annealing chamber, poor basket coiling as a result of entanglement, and the dancer are the major locations where there is frequently occurring wire breakage. The crucial steps in the wire drawing process take place at these locations. The most common faults in the various locations occur due to wire tension as a result of low drawing or annealing solution concentration, entanglement in the basket, inadequate solution flow on dies, bad dies, wire locking in machines, rough surfaces on rollers, annealing bearing failure, improper setting of the drives and tensioner, copper dust in dies, rough surface of contact band, oxidation of wire due to bad steam flow in the annealer, power outages, torque or speed variation due to changes in roll diameter between the payoff drive and the take-up drive, and changing line speed in the drawing stage of the cable, among other factors. Hence, the need to predict the location where faults are likely to occur to help experts easily identify faults when they occur.

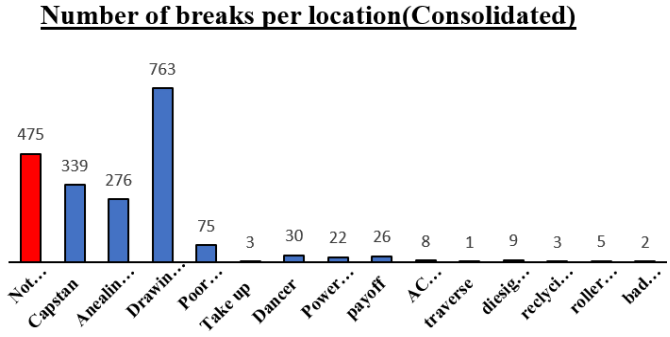

Figure 4
Number of breaks per location

3.3 Trend Analysis

To determine the nature of the data set, a trend analysis was conducted. The linear, exponential and quadratic models was considered. However, the quadratic model was the best among them as shown in Figures 5, 6, 7. Again, a measure of accuracy of the model thus MAPE, MAD and MSD were used as the error metric to determine the model's accuracy. It was discovered that for all the variables considered such as the wire break rate, number of wire breaks and total length the MAD had the least value of 18.47, 0.9311and 47.1 respectively and therefore the best value statistically.

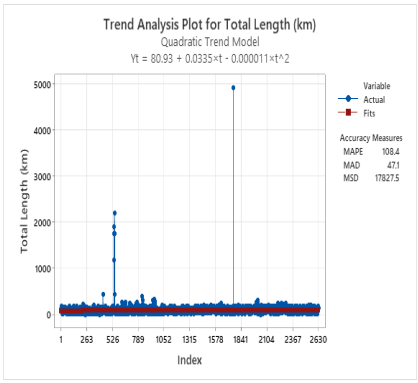

Figure 5
Quadratic trend model for Total Length

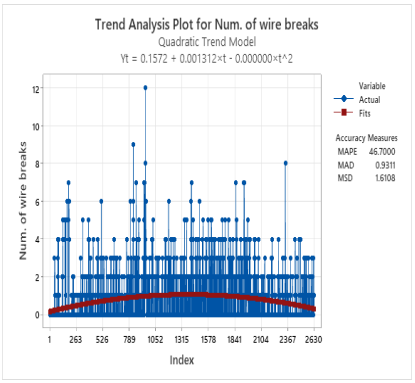

Figure 6
Quadratic trend model for Number of Wire breaks

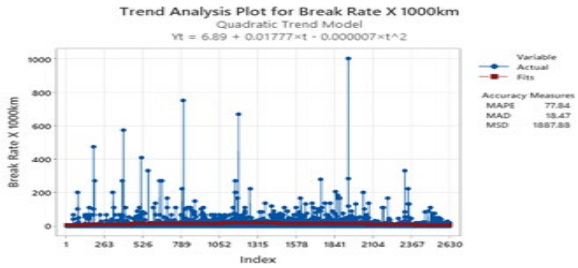

Figure 7
Quadratic trend model for break rate

3.4 Optimal Decision Tree Results

In all, there are four (4) nodes, namely nodes 1 through 4, and four different patterns to achieve an optimal solution as depicted in Figure 8. To achieve an optimal solution based on the mean and standard deviation from the nodes, it could be observed that the system started at node 1 and branched to node 2 and node 4, with a termination at node 4, with a mean and standard deviation of 272.711 and 192.197, respectively. Compared to node 2 and terminal node 4, it can be concluded that node 2 had the optimal values with the least mean and standard deviation of 12.5334 and 36.2605 respectively compared to that of terminal node 4. At terminal node 2, there was another branch to determine an optimal value, namely terminal node 1 and node 3. Finally, at node 3, there was a branch with final termination at terminal nodes 2 and 3. From the analysis, it can be seen that at all the terminal points, terminal node 1 had the best optimal value of 0.546871 and 3.02142, respectively, for the mean and standard deviation. This implies that terminal node 1 is the best model to predict the exact location of the faults during the wire drawing process.

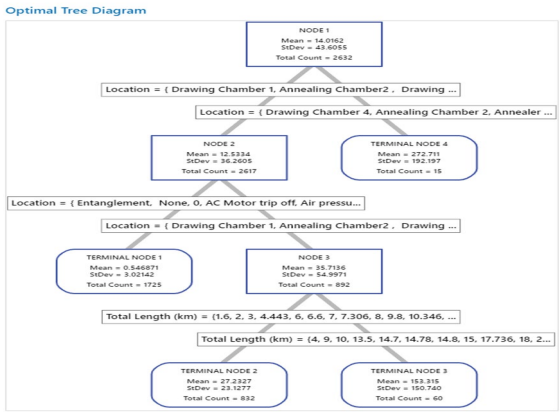

Figure 8
Optimal decision tree diagram

3.5 Hybrid NARNN and Markov Chain Predictive Model

In determining the location of fault during the wire drawing process, the variables that were considered were total length, number of spools, and break rate, and the possible fault locations were the drawing chamber, capstan, payoff, annealing chamber, dancer, bad coiling basket, power outage, winder drive, AC motor trip, and entanglement, with the number of faults recorded in the various locations. Hence, in order to predict the fault occurring within a given location, the NARNN was used to effectively locate the fault condition, as shown in Figure 9. The NARNN diagram was used to determine the pattern of signal in faults per the location in a short time so as to indicate the specific location of faults.

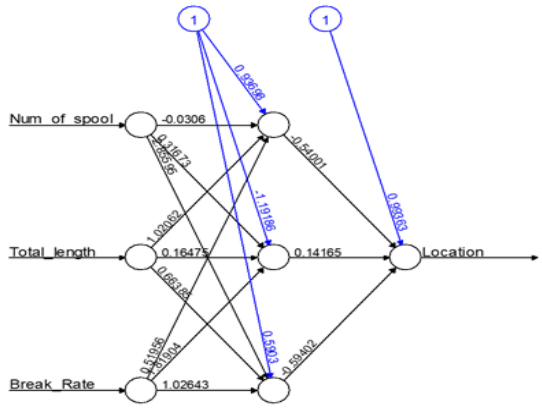

Figure 9
NARNN Predicted Fault Location

To predict the faults from one location to the other based on their transitional probabilities, the Markov chain model was used as shown in Figure 10. This was to determine the probability at which a fault can occur in another location.

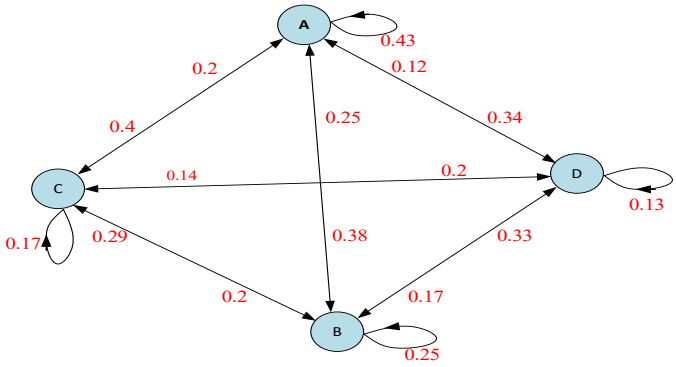

Figure 10
Markov Chain Transitional Probability Diagram

The transitional probability diagram has four pivots, A, B, C, and D, representing the fault locations: drawing chamber, payoff drive, take-up drive, and traverse. The transitional probabilities of fault location occurring at the various pivots are 0.43, 0.25, 0.17, and 0.13, respectively. The transitional probability of a fault from the drawing chamber to the traverse is 0.34, which corresponds to the annealing chamber's transitional probability. Accordingly, there is a 34% likelihood of the fault being located at the annealing chamber from the drawing chamber to the traverse. Once more, the transitional probability of faults from the payoff drive to the take-up drive is 0.29, which matches to the dancer's transitional probability. As a result, there is a 29% possibility that the fault is located at the dancer from the payoff drive to the take-up drive.

Similarly, the transitional probability of faults from the drawing chamber to the payoff drive is 0.38, which represents the transitional probability of the capstan. This indicates that there is a 38% chance that the fault will be found at the capstan linking the drawing chamber to the payoff drive. Additionally, the transitional probability of faults from traverse to payoff drive is 0.17, which is the transitional probability of the recycling system. It translates to a 17% likelihood that the fault will be found at the recycling system between the traverse and the payoff. Furthermore, the diesing chamber's transitional probability, which is given by the transitional probability of faults from the take-up to the traverse, is 0.2. In other words, there is a 20% chance that the fault will be found in the diesing chamber from the take-up to traverse.

These findings are consistent, with distinct transitional probabilities, across different fault locations. Hence, there is a high probability of faults being located at Pivot A, which is the drawing chamber with a high transitional probability. If a

fault is detected in the drawing chamber, it can also damage the annealing chamber, capstan, and dancer, which are essential components of the drawing machine. Therefore, extra attention should be paid to the drawing chamber during the production process to minimize faults from affecting other locations of the drawing machine.

3.6 Predictive Performance Indicators of the Models

Table 2 depicts the performance indicators of the decision tree algorithm and the NARNN. To measure the model's accuracy for the training data using the decision tree, it was observed that the MAPE had the lowest value of 1.2191 and was hence the best model. This was followed by MAD with a value of 8.6312. The RMSE had the highest value of 24.4991, which clearly depicts that the RMSE cannot be considered the best indicator when evaluating the model's accuracy. In the same way, the R-square value recorded using the decision tree was 65.66%, indicating that the model is adequate. The same trend was also observed in the testing.

Again, the training results from the NARNN depict that the MAD had the lowest value of 0.01153, which shows that it is the best indicator for measuring the accuracy of the model. This was closely followed by RMSE with a value of 0.4285496 with the worse indicator among the error metrices being MAPE with a value of 1.250. It was also observed that the testing data mimicked the training data, with MAD and RMSE as the best indicators, respectively. In comparison with the decision tree, it can be deduced that the NARNN had the best model based on the error matrices considered in this study.

Table 2
Error Metric Indicators

Error Metrics	Decision Tree		NARNN	
	Training	Testing	Training	Testing
RMSE	24.4991	43.1110	0.4285496	0.5832
MAD	8.6312	10.7418	0.01153	0.7134
MAPE	1.2191	0.9811	1.2500	2.5312
R-squared	65.66%	17.59%		

3.7 Predicted results of Research Data

Figures 11, 12, 13, and 14 show the predicted graphs of the research variables such as total length, number of wire breaks, number of spools, and break rate for the years 2018 to 2024 based on the NARNN model.

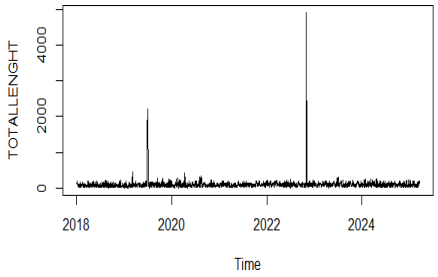

Figure 11
Predicted Results for Total Length

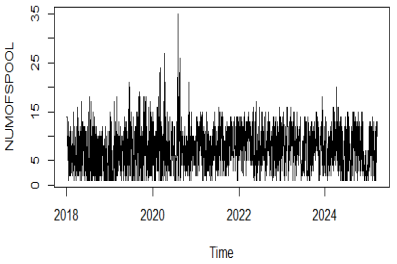

Figure 12
Predicted Results for Number of Spools

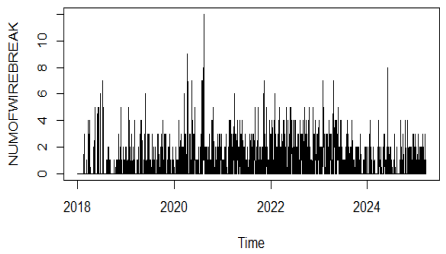

Figure 13
Predicted Results for Number of Wire Breaks

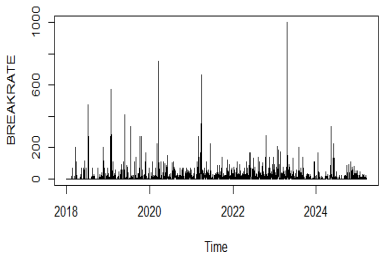

Figure 14
Predicted Results for Wire Break Rate

In summary, the research findings indicate that the hybrid model produced a highly predictive result and smooth transitional probabilities between fault locations when compared to the classical techniques reported in [12], [26], [35], [36].

Conclusions

In summary, the prediction of wire break location during the cable drawing process has been achieved. It was observed that the hybrid NARNN and Markov chain model could effectively predict the break location with higher accuracy when compared to that of the decision tree. One key finding of this research is that no literature has reported on prediction of wire break location in the cable manufacturing industry, and the application of NARNN and the Markov chain model to wire break location prediction further enhances the novelty of this research. It is recommended that cable manufacturers adopt the proposed model for easy fault prediction during the wire drawing process so as to reduce downtime, minimize scrap production, and improve the efficiency and quality of manufactured cables. Subsequent research will center on utilizing machine learning techniques to predict fault locations in copper wire manufacturing.

Acknowledgement

The authors thank Jiangsu University, China for providing the resources needed to finish this research work.

References

[1] Tasevski, G., Petreski, K. A study on the tuner roll impact on the wire drawing process. International journal of industrial engineering and technology, Vol. 6 (2), 2016, pp. 17-22

[2] Verma, S., Sudhakar, R. P. Design and analysis of process parameters on multistage wire drawing process- a review. International journal of mechanical and production engineering research and development, Vol. 9(1), 2019, pp. 403-412

[3] Ofosu, R. A., Normanyo, E., Obeng, L. Temperature control of heaters in cable extrusion machine using PSO-ANFIS controller. In proceedings of IEEE AFRICON Conference, 2019, pp. 1-9

[4] Larsson, J., Jansson, A., Karlsson, P. Monitoring and evaluation of the wire drawing process using thermal imaging. International journal of advanced manufacturing technology, Vol. 3, 2018, pp. 1-14

[5] Mahto, P. K., Murmu, R. Temperature control for plastic extrusion process. International journal of innovative research in science, engineering and technology, Vol. 4(7), 2015, pp. 5748-5758

[6] Jie-Shiou, L., Ming-Yang, C., Ke-Han, S., Mi-Chi, T. Wire tension control of an automatic motor winding machine-an iterative learning sliding mode control approach. Robotics and computer–integrated manufacturing, Vol. 50, 2018, pp. 50-62

[7] Perduková, D., Fedor, P., Fedák, V., Padmanaban, S. Lyapunov based reference model of tension control in a continuous strip processing line with multi-motor drive. Electronics, Vol. 8 (60), 2019, pp. 1-24

[8] Zhewei, G., Sheng, Z., Kaijie, Z., Chenliang, S. Fully-digital tension control system with PID algorithm for winding ultrafine enameled wires. In IOP Conference Series: Materials Science and Engineering, Vol. 892, 2020, p. 012064

[9] Huang, P. Y., Cheng, M. Y., Su, K. H., Kuo, W. L. Control of roll-to-roll manufacturing based on sensorless tension estimation and disturbance compensation. Journal of the chinese institute of engineers, Vol. 44(2), 2021, pp. 89-103

[10] Li, Y., Wang, Z., Zhe, L., Jiang, Z. Research on Fault Prognosis Methods Based on Data-driven : A Survey. In IOP Conference Series: Materials Science and Engineering, Vol. 1043, 2021, p. 042008

[11] Xing, D., Haijian, S., Chunlong, H., Dengbiao, J., Yingtao, J. Wind power forecasting methods based on deep learning: A Survey. Computer Modeling in Engineering and Sciences, Vol. 122(1), 2020, pp. 273-301

[12] Pereira, F. H., Bezerra, F. E., Shigueru, J., Josemir, S., Chabu, I., de Souza, G. F. M., Micerino, F., Nabeta, S. I. Nonlinear autoregressive neural

network models for prediction of transformer oil-dissolved gas concentrations. Energies, Vol. 11(7), 2018, pp. 1-12

[13] Shao, H., Deng, X., Jiang, Y. A novel deep learning approach for short-term wind power forecasting based on infinite feature selection and recurrent neural network. Journal of renewable and sustainable energy, Vol. 10, 2018, pp. 1-12

[14] Fernandes, M., Corchado, J. M., Marreiros, G. Machine learning techniques applied to mechanical fault diagnosis and fault prognosis in the context of real industrial manufacturing use-cases: a systematic literature review. Applied Intelligence, Vol. 52, 2022, pp. 14246-14280

[15] Cheng, L., Yu, T. Dissolved gas analysis principle-based intelligent approaches to fault diagnosis and decision making for large oil-immersed power transformers: A Survey. Energies, Vol. 2018(11), 2018, pp. 1-13

[16] Radu-Emil, P., Claudia-Adina, B. D., Elena-Lorena, H., Raul-Cristian, R., Emil, M. P. Evolving fuzzy models of shape memory alloy wire actuators, Romanian Journal of Information Science And Technology. Vol. 24(4), 2021, 353-365

[17] Radu-Emil, P., Gheorghe, D., Sergey, T., Inga, Z. Processing, neural network-based modeling of biomonitoring studies data and validation on republic of moldova data. In the Romanian Academy, Series A-Mathematics Physics Technical Sciences Information Science. Vol. 23(4), 2022, pp. 403-410

[18] Shahnaz, N. S., Dursun, E. An input-weighted, multi-objective evolutionary fuzzy classifier, for alcohol classification. Acta Polytechnica Hungarica. Vol. 197(10), 2022, 61-81

[19] Ofosu, R. A., Asiedu-Asante, A. B., Adjei, R. B. Fuzzy logic based condition monitoring of a 3-phase induction motor. In proceedings of IEEE AFRICON 2019, pp. 1-8

[20] Blanchard, T., Samanta, B. Wind speed forecasting using neural networks. Wind Engineering, Vol. 44(1), 2020, pp. 33-48

[21] Mihalache, S., Burileanu, D. Speech emotion recognition using deep neural networks, transfer learning and ensemble classification techniques. Romanian Journal of Information, Science and Technology, Vol. 26 (3-4), 2023, pp. 375-387

[22] Li, Z., Wang, Y., Wang, K. S. Intelligent predictive maintenance for fault diagnosis and prognosis in machine centers: Industry 4.0 scenario. Advances in Manufacturing, Vol. 5(4), 2017, pp. 377-387

[23] Ruiz, L. G. B., Cuéllar, M. P., Calvo-Flores, M. D., Jiménez, M. D. C. P. An application of non-linear autoregressive neural networks to predict

energy consumption in public buildings. Energies, Vol. 2016,(9), 2016, pp. 1-21

[24] De Giorgi, M. G., Ficarella, A., Quarta, M. Dynamic performance simulation and control of an aeroengine by using NARX models. In Proceedings of MATEC Web conference, Vol. 304, 2019, pp. 1-8

[25] Chatterjee, S., Nigam, S., Singh, J. B., Upadhyaya, L. N. Software fault prediction using Nonlinear Autoregressive with eXogenous Inputs (NARX) network. Applied Intelligence, Vol. 37, 2012, pp. 21-129

[26] Nistane, V. M. Wavelet-based features for prognosis of degradation in rolling element bearing with non-linear autoregressive neural network. Australian Journal of Mechanical Engineering, Vol. 19(4), 2021, pp. 423-437

[27] Umit, K., Esra, S. E., Mumine, K. K. Binary anarchic society optimization for feature selection. Romanian Journal of Information Science and Technology, Vol. 26 (3-4), 2023, pp. 351-364

[28] Suvendu, M., Swarup, P., Soudip, H. Artificial neural network coupled condition monitoring for advanced fault diagnosis of engine. Research square, 2021, pp. 1-40

[29] Zajacko, I., Kuric, I., Gal, T. Application of machine learning for failure prediction in manufacturing process. In Proceedings of ISSAT International Conference on Data Science and Intelligent Systems, 2019, pp. 1-5

[30] Ren, G., Gao, J. Comparison of NARNN and ARIMA models for short-term metro passenger flow forecasting. In 19th COTA International Conference of Transportation Professionals, 2019, pp. 1352-1361

[31] Huang, J. F., Lu, W. C. Forecasting of meteorological time series and pricing of weather index rainbow options: A wavelet-NAR neural network model. Systems Engineering-Theory and Practice, Vol. 36(5), 2016, pp. 1146-1154

[32] Adil, A., Muhammad, K. Multi-step ahead wind forecasting using nonlinear autoregressive neural networks. Energy Procedia, Vol. 134, 2017, pp. 192-204

[33] Islam, M. P., Morimoto, T. Non-linear autoregressive neural network approach for inside air temperature prediction of a pillar cooler. International Journal of Green Energy, Vol. 14, 2017, pp. 41-149

[34] Caswell, J. M. A Nonlinear autoregressive approach to statistical prediction of disturbance storm time geomagnetic fluctuations using solar data. Journal of Signal and Information Processing, Vol. 5, 2014, pp. 42-53

[35] Namasudra, S., Dhamodharavadhani, S., Rathipriya, R. Nonlinear neural network based forecasting model for predicting COVID-19 cases. Neural Processing Letters, Vol. 55, 2023, pp. 171-191

[36] Vanfretti, L., Arava, V. S. N. Decision tree-based classification of multiple operating conditions for power system voltage stability assessment. International Journal of Electrical Power and Energy Systems, Vol. 123, 2020, pp. 1-10

[37] Ioan-Daniel, B., Radu-Emil, P., Alexandra-Bianca, B. Improvement of k-means cluster quality by post processing resulted clusters. Procedia Computer Science, Vol. 199, 2022, pp. 63-70

[38] Arican, E., Aydin, T. An RGB-D descriptor for object classification. Romanian Journal of Information Science and Technology, Vol. 25 (3-4), 2022, pp. 338-349

[39] Zhou, Y., Wang, Y., Zhong, L., Tan, R. A markov chain based demand prediction model for stations in bike sharing systems. Mathematical Problems in Engineering, Vol. 2018, 2018, pp. 1-8

[40] Ong, K., Sugiura, B. T., Zettsu, K. Dynamically pre-trained deep recurrent neural networks using environmental monitoring data for predicting PM2.5. Neural computing and applications. Vol. 27, 2016, pp. 1553-1566

[41] Ofosu, R. A., Odoi, B., Asamoah, M. Electricity consumption forecast for tarkwa using autoregressive integrated moving average and adaptive neuro fuzzy inference system. Serbian Journal of Electrical Engineering, Vol. 18(1), 2021, pp. 75-94

[42] Twumasi-Ankrah, Sampson., Odoi, B., Adoma, W. P, Gyamfi, H. E. Efficiency of imputation techniques in univariate time series. International Journal of Science, Environment, and Technology, Vol. 8(3) 2019, pp. 430-453